NASA TN D-1608

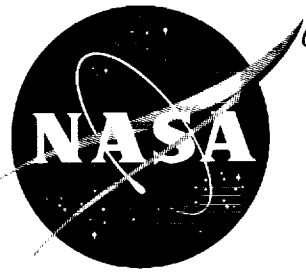

TECHNICAL NOTE

D-1608

AN ANALYTICAL STUDY OF A SIMPLE ATTITUDE CONTROL SYSTEM FOR A FINNED VEHICLE

By Jack E. Harris

Langley Research Center
Langley Station, Hampton, Va.

NATIONAL AERONAUTICS AND SPACE ADMINISTRATION
WASHINGTON
March 1963

SINGLE COPY ONLY

NATIONAL AERONAUTICS AND SPACE ADMINISTRATION

TECHNICAL NOTE D-1608

AN ANALYTICAL STUDY OF A SIMPLE ATTITUDE CONTROL SYSTEM FOR A FINNED VEHICLE

By Jack E. Harris

SUMMARY

An analytical study was made of a finned-vehicle first-stage attitude control system incorporating an attitude error feedback signal and simple forward-loop compensation. The effects of various compensation networks on system performance are compared for flight conditions, ranging from dynamic pressures of 100 lb/sq ft to 3,200 lb/sq ft. A simple tandem compensation network that enables the control system to obtain good response characteristics to attitude command inputs and to maintain satisfactory path control when subjected to wind disturbance is discussed.

INTRODUCTION

Finned vehicles often are used for space-probe missions. High pointing accuracies are seldom required, and by spinning the vehicle about its longitudinal axis, thrust misalinements that could cause tumbling are channeled into the production of gyroscopic precession and nutation. The amplitude of these gyroscopic motions is dependent on spin rate, and therefore the deviation of the longitudinal axis of the vehicle from a prescribed spatial direction can be kept small. However, the wind shears encountered during transition through atmosphere can produce disturbances that cause too large a path deviation, and a more positive spatial orientation of the vehicle is required, especially for finned vehicles. This paper presents the results of an analytical study of the feasibility of using a simple first-stage control system, incorporating an attitude signal as the only feedback loop, in order to control the attitude of a vehicle traversing the more dense areas of the atmosphere. The specific task was to afford control of a fin-stabilized solid-fuel vehicle during the first 40 seconds of flight. After this time interval, the vehicle would be spun up and rely upon spinning to maintain its proper attitude.

The results of the study are presented in terms of root-locus plots which show the effect of various compensating networks on the system characteristics, and transient-response plots which show the attitude response of the vehicle to input commands and its resistance to external disturbances.

The effects of the first three bending modes on system stability are considered in the analysis since system instability can sometimes be caused by coupling between control modes and structural modes.

SYMBOLS

$B(s)$	feedback signal proportional to vehicle attitude
$C_{L,j}$	local lift coefficient at jth station
$d_{i,j}$	normalized displacement of ith bending mode at jth station, positive in lift direction, ft/ft
$d_{i,T}$	normalized displacement of ith bending mode at nozzle exit, ft/ft
$d_{i,\delta}$	normalized displacement of ith bending mode at control surface center of pressure, ft/ft
$E(s)$	control-system forward-loop error signal
F_δ	jet-vane lift force per unit control deflection, lb/degree
F_Z	force input to translation mode, positive downward, lb
$G(s)$	frequency-dependent terms of transfer function particularized by the numerical subscript
h_i	displacement of reference point to which ith mode is normalized, ft
i	bending mode
I_Y	moment of inertia about the Y-axis, ft-lb/sec^2
j	body station
$j\omega$	imaginary portion of the complex variable $s = \sigma \pm j\omega$, radians/sec
K	static gain of transfer function particularized by the numerical subscript
K_V	loop root locus gain
L	lift force, positive upward, lb
M_Y	pitching moment about Y-axis, positive for nose up, ft-lb
m	total mass of vehicle, slugs

m_i	generalized mass of ith mode, slugs
n	integer
Q_i	generalized force input to ith bending mode, positive upward, lb
q	dynamic pressure, lb/ft^2
R(s)	reference input command, proportional to desired vehicle attitude
r(t)	reference input command
S	lift coefficient reference area, area of base diameter, ft^2
s	Laplace operator, per sec
T	thrust in pounds
t	time
V	velocity along flight path, ft/sec
X,Y,Z	orthogonal principal body axes
$\bar{x}_j$	distance from body station j to center of gravity of the vehicle, positive if station is forward of center of gravity, ft
$\bar{x}_T$	distance from nozzle exit to vehicle center of gravity, ft
$\bar{x}_\delta$	distance from control surface center of pressure to vehicle center of gravity, ft
α	rigid-body angle of attack, degrees or radians
α_j	local angle of attack at jth station, degrees or radians
δ	control deflection, degrees or radians
ζ_i	structural damping ratio of ith mode
θ	rigid-body angular displacement about the Y-axis, degrees or radians
θ_G	angular displacement about the Y-axis at sensor location, degrees or radians
$\lambda_{i,G}$	slope of normalized mode i at sensor location, radians/ft
$\lambda_{i,T}$	slope of normalized mode i at nozzle exit, radians/ft
σ	real portion of the complex variable $s = \sigma \pm j\omega$, sec^{-1}

ϕ angular displacement about the X-axis, degrees or radians

ψ angular displacement about the Z-axis, degrees or radians

ω_i natural frequency of ith mode, radians/sec

A dot over quantity indicates the differentiation with respect to time; a double dot indicates the second differentiation with respect to time.

A subscript to a subscript denotes the derivative of the quantity represented by the principal symbol, with respect to the quantity related to the second subscript. For example:

$$\left(C_{L_\alpha}\right)_j = \frac{\partial C_{L,j}}{\partial \alpha_j} \text{ per radian}$$

SYSTEM AND VEHICLE CHARACTERISTICS

The vehicle characteristics used in this study are representative of the NASA Scout, a four-stage solid-fuel vehicle. The first stage is controlled by movable aerodynamic tip fins and jet vanes immersed in the first-stage motor exhaust. These surfaces are positioned by a hydraulic servosystem, normally positioned in proportion to the sum of vehicle attitude and rate error signals. The system incorporated in this study, however, utilized only an attitude-error signal. The system studied is shown in block diagram form in figure 1. The servoactuator, attitude gyroscope, compensating network, and airframe transfer functions used in this study are listed in table I. The approximation of the servo and gyro components by first-order time lags was believed to be sufficient for this investigation. The manner in which the airframe transfer functions were obtained will be discussed subsequently.

A sketch of the vehicle used in this study is shown in figure 2. The configuration and the specific station numbering convention used herein are shown in figure 2(a), and the axis system employed is shown in figure 2(b).

ANALYSIS AND DISCUSSION

Equations and Determination of the Transfer Function

For purposes of analysis, the aerodynamic force inputs were assumed to act at force stations at the nose (station 15), at the flares between the third and fourth stages (station 125), between the first and second stages (station 470), and at the center of pressure of the fin. This assumption is consistent with slender-body theory. The actual lift distribution is dependent upon the local angles of attack along the body, and these in turn are affected by the bending. Thus, a complete description of the vehicle airframe can be obtained by using the

normal rigid-body equations of motion in conjunction with a set of wave equations for the body. The small perturbation equations for the longitudinal plane can be written as follows (ref. 1):

Normal translation -

$$mV(\dot{\theta} - \dot{\alpha}) = -F_Z \tag{1}$$

Pitch -

$$I_Y\ddot{\theta} = M_Y \tag{2}$$

Bending modes -

$$m_i\ddot{h}_i = Q_i(i = 1,2,3) \tag{3}$$

An auxiliary equation for the attitude at a sensor location is given by

$$\theta_G = \theta + 57.3\sum_{i=1}^{3} \lambda_{i,G}h_i \tag{4}$$

The forces and moments (ref. 2) acting on the vehicle can be defined as:

$$F_Z = -\sum_{j=1}^{4} \left[\left(C_{L_\alpha}\right)_j \alpha_j qS\right] - \left[\left(C_{L_\delta}\right)_j qS + F_\delta\right]\delta - T\left(\alpha + \sum_{i=1}^{3} \lambda_{i,T}h_i\right) \tag{5}$$

$$M_Y = \sum_{j=1}^{4} \left[\left(C_{L_\alpha}\right)_j \bar{x}_j\alpha_j qS\right] + \left[\left(C_{L_\delta}\right)_j qS + F_\delta\right]\bar{x}_\delta\delta + T\sum_{i=1}^{3} \left(\bar{x}_T\lambda_{i,T} - d_{i,T}\right)h_i \tag{6}$$

$$Q_i = \sum_{j=1}^{4} \left[\left(C_{L_\alpha}\right)_j \alpha_j qSd_{i,j}\right] + \left[\left(C_{L_\delta}\right)_j qS + F_\delta\right]d_{i,\delta}\delta - m_i\left(\omega_i{}^2h_i + 2\zeta_i\omega_i\dot{h}_i\right) \tag{7}$$

where

$$\alpha_j = \alpha - \frac{\bar{x}_j\dot{\theta}}{V} + \sum_{i=1}^{3} \left(\lambda_{i,j}h_i\right) - \sum_{i=1}^{3} \frac{d_{i,j}\dot{h}_i}{V} \tag{8}$$

Substituting equation (8) into equations (5), (6), and (7) leads to the following set of simultaneous differential equations of motion in Laplace notation:

$$\begin{bmatrix} -s + \frac{F_{Z_\alpha}}{V} & s & \frac{F_{Z_{\dot{h}_1}}}{V}s + \frac{F_{Z_{h_1}}}{V} & \frac{F_{Z_{\dot{h}_2}}}{V}s + \frac{F_{Z_{h_2}}}{V} & \frac{F_{Z_{\dot{h}_3}}}{V}s + \frac{F_{Z_{h_3}}}{V} \\ M_\alpha & -s^2 + M_{\dot{\theta}}s & M_{\dot{h}_1}s + M_{h_1} & M_{\dot{h}_2}s + M_{h_2} & M_{\dot{h}_3}s + M_{h_3} \\ Q_{1_\alpha} & Q_{1_{\dot{\theta}}}s & -s^2 + Q_{1_{\dot{h}_1}}s + Q_{1_{h_1}} & Q_{1_{\dot{h}_2}}s + Q_{1_{h_2}} & Q_{1_{\dot{h}_3}}s + Q_{1_{h_3}} \\ Q_{2_\alpha} & Q_{2_{\dot{\theta}}}s & Q_{2_{\dot{h}_1}}s + Q_{1_{h_2}} & -s^2 + Q_{2_{\dot{h}_2}}s + Q_{2_{h_2}} & Q_{2_{\dot{h}_3}}s + Q_{2_{h_3}} \\ Q_{3_\alpha} & Q_{3_{\dot{\theta}}}s & Q_{3_{\dot{h}_1}}s + Q_{3_{h_1}} & Q_{3_{\dot{h}_2}}s + Q_{3_{h_2}} & -s^2 + Q_{3_{\dot{h}_3}}s + Q_{2_{h_3}} \end{bmatrix} \begin{bmatrix} \alpha \\ \theta \\ h_1 \\ h_2 \\ h_3 \end{bmatrix} = \delta \begin{bmatrix} -\frac{F_{Z_\delta}}{V} \\ -M_\delta \\ -Q_{1_\delta} \\ -Q_{2_\delta} \\ -Q_{3_\delta} \end{bmatrix} \tag{9}$$

The coefficients used in this matrix are defined in appendix A. Aerodynamic loading, structural mode-shape data, as well as center-of-pressure and center-of-gravity locations as functions of time were obtained from references 3 and 4. Other parameter data were also obtained from these references.

Equation (9) was solved in conjunction with equation (4) to obtain the vehicle transfer function relating the change in attitude at the sensor location to a change in the control deflections by using the matrix coefficients associated with four flight conditions along the trajectory shown in figure 3. These flight conditions consisted of a time shortly after lift-off (5 seconds) chosen because of the low short-period damping and low control effectiveness that exist at that time; a moderate dynamic-pressure condition just prior to entering the transonic region (15 seconds), chosen because of the rapid change that takes place in several of the coefficients; maximum dynamic-pressure condition (32.5 seconds), chosen because of the large control effectiveness available at that point; and a condition just prior to spin-up (40 seconds).

By combining the airframe transfer function with the transfer functions of the other system components, the following closed-loop system function can be obtained:

$$\frac{\theta_G(s)}{R(s)} = \frac{K_1G_1(s)\ K_2G_2(s)\ K_3G_3(s)}{1 + K_1G_1(s)\ K_2G_2(s)\ K_3G_3(s)\ K_4G_4(s)} \tag{10}$$

By equating the closed-loop function denominator to zero and solving this equation, a plot of the variations of the poles (hence, the natural response characteristics) of the closed-loop system with changes in the open-loop gain for any particular numerical set of coefficients of the motion-equation matrix can be obtained.

Because of the importance of the vehicle response to wind, the effects of gust penetration were also investigated. For purposes of analysis, the wind gust can be considered to act as a step change in angle of attack. The equation defining the local angle of attack (eq. (8)) can be rewritten to include a gust angle in the following manner:

$$\alpha_j = \alpha + \alpha_g - \frac{\bar{x}_j \dot{\theta}}{V} + \sum_{i=1}^{3} \left(\lambda_{i,j} h_i\right) - \sum_{i=1}^{3} \frac{d_{i,j} \dot{h}_i}{V} \tag{11}$$

where α_g is the gust angle. The relationship between this angle and the horizontal wind is given by

$$\alpha_g = \tan^{-1} \frac{u_n}{V_v} \tag{12}$$

where u_n is the horizontal wind velocity and V_v is the vertical velocity of the vehicle.

Equation (9) was rewritten by considering α_g as a forcing function, and the pitch matrix was solved by considering the controls locked to obtain a $\theta_G(s)/\alpha_g(s)$ transfer function. The block diagram shown in figure 1 was redrawn to consider a disturbance input $\left(\alpha_g\right)$ acting on the airframe plus a zero reference input command to the entire system.

The output transient response equation can be obtained graphically from the roots of the partial fraction expansion of the new open-loop equation. The value of the denominator roots will be closed-loop values obtained from the original solution of equation (9); however, the numerator roots are changed as a result of the disturbance.

Attitude gyros as a rule have considerable drift rates which may introduce an appreciable error in the flight path. Since the proposed control utilizes only attitude gyros as the reference elements, a determination of the errors that might be introduced is required. The calculation of these errors is presented in appendix B.

Presentation of Results

As seen in table I, the airframe transfer function $\theta_G(s)/\delta(s)$ is characterized in the complex (s) plane by a dipole consisting of an integration pole and a first-order zero located near the origin plus the complex poles of the short-period and bending modes. In closed-loop operation, finite values of loop gain cause the integration pole to move away from its origin location toward the airframe zero. This movement results in the introduction of a decaying exponential term whose contribution to the system's transient response is normally of a

reductive nature. The pole's motion with increasing loop gain (toward the zero) is such as to diminish the magnitude of its effect and to reduce the time its contribution is noticeable. Thus, the higher the system loop gain, the less noticeable this term becomes. High loop gain, however, introduces instability into the system through a reduction in the effective structural damping associated with the first bending mode. Some compromise must be made, and the following work indicates the steps taken in making this compromise.

In the interest of simplicity, it was felt that a modification could be made to the network presently incorporated in the Scout. This network consists of a lag-lag network with poles located at -29 and -33 nepers per second in the complex plane. Since it was felt that some anticipation would be required to replace that obtained in the basic vehicle by means of rate feedback, several lead terms were considered in connection with the basic lag-lag network. Three lead terms plus a lead-lag term were investigated in this study.

Figure 4 shows the root loci of the variation in the system structural and elastic characteristics as a function of open-loop gain at each of three flight conditions with the compensation network $G_{1,1}(s)$ in the forward loop. The second and third bending modes are not shown on the figure, but were included in the analysis. Their motion as a function of gain was negligible over the gain range investigated. The limiting case from a stability standpoint was found to be the maximum dynamic pressure case (fig. 4(c)). Both minimum ($K_V \leqq 0.32$) and maximum ($K_V \geqq 6$) usable gain values exist for this flight condition. At times greater than 35 seconds after launch, the system is inherently stable again. However, no loci are shown for any of these stable conditions in this paper. A loop gain of 4 appeared to produce an adequate increase in short-period damping over the range of conditions investigated but did not cause undue degradation in the first bending mode damping. Transient-response plots of the system's response to a step input command incorporating this particular network as well as the other are shown subsequently.

Root loci for other networks were obtained for the same three flight conditions shown in figure 4. No significant improvement was obtained by using either of the networks $G_{1,2}(s)$ or $G_{1,3}(s)$.

Figure 5 presents the root loci for the system when the $G_{1,4}(s)$ compensation network is inserted in series with the system. A loop gain of 32 was arbitrarily chosen as a proper operating value over the range of flight conditions.

Figures 6(a) through 6(d) show the transient response to a step input of the overall system incorporating each of the four networks at several flight conditions and a specific value of loop gain adjudged to be adequate for the particular system configuration. It should be mentioned that the curves represent faired values of the equations underneath them, and thus some of the small-amplitude high-frequency oscillations indicated by the equations are not evidenced by the curves; however, the basic shape of the response is indicated. Notice that in the first three 15-seconds-after-launch cases, the output does not steady upon a value equivalent to the input within the time interval shown, in fact, it does not even maintain 90 percent of the desired value. Also the output slightly

exceeds the input for the first three high dynamic-pressure cases during the time interval shown in the plots. Transient responses associated with network $G_{1,4}(s)$ indicate that the output is maintained within 10 percent of the desired value within $4\frac{1}{2}$ seconds for the 15-seconds-after-launch case and steadies on a value equal to the input within $2\frac{1}{2}$ seconds for the 32.5-second case.

Figure 7 shows several of the transient-response curves associated with a unit-step wind disturbance. Curves were obtained for each of the conditions shown in figure 6; however, only three are shown here for comparison purposes. Notice that the network that afforded the highest command control $G_{1,4}(s)$ also tended to minimize the amount the vehicle was displaced by a disturbance. The control system countered the disturbance quickly enough to limit the maximum vehicle displacement to less than 40 percent of the potential disturbance value and to eliminate 90 percent of the disturbance within 5 seconds.

CONCLUDING REMARKS

It is felt that this analysis, though somewhat limited, has demonstrated the feasibility of removing the rate gyro feedback loop in the control guidance and using an attitude error feedback signal plus forward-loop compensation for probe-type missions with the Scout vehicle. It also indicated that the system possessed sufficiently high forward-loop gain margin; that is, a gain value that offered sufficient speed of response did not cause structural instability.

Langley Research Center,
National Aeronautics and Space Administration,
Langley Station, Hampton, Va., November 20, 1962.

APPENDIX A

DEFINITIONS OF DIMENSION DERIVATIVES

Normal Translation

$$\frac{F_{Z_\alpha}}{V} = \frac{-qS}{mV}\left[\sum_{j=1}^{4}\left(C_{L_\alpha}\right)_j\right] - \frac{T}{mV}$$

$$\frac{F_{Z_{\dot{h}_1}}}{V} = \frac{qS}{mV^2}\left[\sum_{j=1}^{4}\left(C_{L_\alpha}\right)_j d_{1,j}\right]57.3$$

$$\frac{F_{Z_{h_1}}}{V} = -\left\{\frac{qS}{mV}\left[\sum_{j=1}^{4}\left(C_{L_\alpha}\right)_j \lambda_{1,j}\right] + \frac{T}{mV}\lambda_{1,T}\right\}57.3$$

$$\frac{F_{Z_{\dot{h}_2}}}{V} = \frac{qS}{mV^2}\left[\sum_{j=1}^{4}\left(C_{L_\alpha}\right)_j d_{2,j}\right]57.3$$

$$\frac{F_{Z_{h_2}}}{V} = -\left\{\frac{qS}{mV}\left[\sum_{j=1}^{4}\left(C_{L_\alpha}\right)_j \lambda_{2,j}\right] + \frac{T}{mV}\lambda_{2,T}\right\}57.3$$

$$\frac{F_{Z_{\dot{h}_3}}}{V} = \frac{qS}{mV^2}\left[\sum_{j=1}^{4}\left(C_{L_\alpha}\right)_j d_{3,j}\right]57.3$$

$$\frac{F_{Z_{h_3}}}{V} = -\left\{\frac{qS}{mV}\left[\sum_{j=1}^{4}\left(C_{L_\alpha}\right)_j \lambda_{3,j}\right] + \frac{T}{mV}\lambda_{3,T}\right\} 57.3$$

$$\frac{F_{Z_\delta}}{V} = \frac{-qS}{mV}\left(C_{L_\delta}\right)_j - \frac{F_\delta}{mV} 57.3$$

First Bending Mode

$$Q_{1_\alpha} = \frac{qS}{m_1}\left[\sum_{j=1}^{4}\left(C_{L_\alpha}\right)_j d_{1,j}\right]\frac{1}{57.3}$$

$$Q_{1_{\dot\theta}} = \frac{-qS}{m_1 V}\left[\sum_{j=1}^{4}\left(C_{L_\alpha}\right)_j \bar{x}_j\, d_{1,j}\right]\frac{1}{57.3}$$

$$Q_{1_{\dot h_1}} = -2\zeta_1\omega_1 - \frac{qS}{m_1 V}\left[\sum_{j=1}^{4}\left(C_{L_\alpha}\right)_j d_{1,j}^2\right]$$

$$Q_{1_{h_1}} = -\omega_1^2 + \frac{qS}{m_1}\left[\sum_{j=1}^{4}\left(C_{L_\alpha}\right)_j \lambda_{1,j}\, d_{1,j}\right]$$

$$Q_{1_{\dot h_2}} = \frac{-qS}{m_1 V}\left[\sum_{j=1}^{4}\left(C_{L_\alpha}\right)_j d_{1,j}\, d_{2,j}\right]$$

$$Q_{1_{h_2}} = \frac{qS}{m_1}\left[\sum_{j=1}^{4}\left(C_{L_\alpha}\right)_j\ d_{1,j}\lambda_{2,j}\right]$$

$$Q_{1_{\dot{h}_3}} = \frac{-qS}{m_1 V}\left[\sum_{j=1}^{4}\left(C_{L_\alpha}\right)_j\ d_{1,j}\ d_{3,j}\right]$$

$$Q_{1_{h_3}} = \frac{qS}{m_1}\left[\sum_{j=1}^{4}\left(C_{L_\alpha}\right)_j\ d_{1,j}\lambda_{3,j}\right]$$

$$Q_{1_\delta} = \frac{qS}{m_1}\left(C_{L_\delta}\right)_j\ d_{1,\delta}\ \frac{1}{57.3} + \frac{F_\delta\ d_{1,\delta}}{m_1}$$

Second Bending Mode

$$Q_{2_\alpha} = \frac{qS}{m_2}\left[\sum_{j=1}^{4}\left(C_{L_\alpha}\right)_j\ d_{2,j}\right]\frac{1}{57.3}$$

$$Q_{2_{\dot{\theta}}} = \frac{-qS}{m_2 V}\left[\sum_{j=1}^{4}\left(C_{L_\alpha}\right)_j\ \bar{x}_j\ d_{2,j}\right] = \frac{1}{57.3}$$

$$Q_{2_{\dot{h}_1}} = \frac{-qS}{m_2 V}\left[\sum_{j=1}^{4}\left(C_{L_\alpha}\right)_j\ d_{2,j}\ d_{1,j}\right]$$

$$Q_{2_{h_1}} = \frac{qS}{m_2}\left[\sum_{j=1}^{4}\left(C_{L_\alpha}\right)_j d_{2,j}\lambda_{1,j}\right]$$

$$Q_{2_{\dot{h}_2}} = -2\zeta_2\omega_2 - \frac{qS}{m_2V}\left[\sum_{j=1}^{4}\left(C_{L_\alpha}\right)_j d_{2,j}^2\right]$$

$$Q_{2_{h_2}} = -\omega_2^2 + \frac{qS}{m_2}\left[\sum_{j=1}^{4}\left(C_{L_\alpha}\right)_j d_{2,j}\lambda_{2,j}\right]$$

$$Q_{2_{\dot{h}_3}} = \frac{-qS}{m_2V}\left[\sum_{j=1}^{4}\left(C_{L_\alpha}\right)_j d_{2,j}\, d_{3,j}\right]$$

$$Q_{2_{h_3}} = \frac{qS}{m_2}\left[\sum_{j=1}^{4}\left(C_{L_\alpha}\right)_j d_{2,j}\lambda_{3,j}\right]$$

$$Q_{2_\delta} = \frac{qS}{m_2}\left(C_{L_\delta}\right)_j d_{2,\delta}\frac{1}{57.3} + \frac{F_\delta\, d_{2,\delta}}{m_2}$$

Third Bending Mode

$$Q_{3_\alpha} = \frac{qS}{m_3}\left[\sum_{j=1}^{4}\left(C_{L_\alpha}\right)_j d_{3,j}\right]\frac{1}{57.3}$$

$$Q_{3_{\dot{\theta}}} = \frac{-qS}{m_3 V}\left[\sum_{j=1}^{4}\left(C_{L_\alpha}\right)_j \bar{x}_j\, d_{3,j}\right]\frac{1}{57.3}$$

$$Q_{3_{\dot{h}_1}} = \frac{-qS}{m_3 V}\left[\sum_{j=1}^{4}\left(C_{L_\alpha}\right)_j d_{1,j}\, d_{3,j}\right]$$

$$Q_{3_{h_1}} = \frac{qS}{m_3}\left[\sum_{j=1}^{4}\left(C_{L_\alpha}\right)_j \lambda_{1,j}\, d_{3,j}\right]$$

$$Q_{3_{\dot{h}_2}} = \frac{-qS}{m_3 V}\left[\sum_{j=1}^{4}\left(C_{L_\alpha}\right)_j d_{2,j}\, d_{3,j}\right]$$

$$Q_{3_{h_2}} = \frac{qS}{m_3}\left[\sum_{j=1}^{4}\left(C_{L_\alpha}\right)_j \lambda_{2,j}\, d_{3,j}\right]$$

$$Q_{3_{\dot{h}_3}} = -2\zeta_3\omega_3 - \frac{qS}{m_3 V}\left[\sum_{j=1}^{4}\left(C_{L_\alpha}\right)_j d_{3,j}^2\right]$$

$$Q_{3_{h_3}} = -\omega_3^2 + \frac{qS}{m_3}\left[\sum_{j=1}^{4}\left(C_{L_\alpha}\right)_j d_{3,j}\lambda_{3,j}\right]$$

$$Q_{3_\delta} = \frac{qS}{m_3}\left(C_{L_\delta}\right)_j \, d_{3,\delta} \, \frac{1}{57.3} + \frac{F_\delta \, d_{3,\delta}}{m_3}$$

Pitch

$$M_\alpha = \frac{qS}{I_Y}\left[\sum_{j=1}^{4} \left(C_{L_\alpha}\right)_j \, \bar{x}_j\right]$$

$$M_{\dot{\theta}} = \frac{-qS}{VI_Y}\left[\sum_{j=1}^{4} \left(C_{L_\alpha}\right)_j \, \bar{x}_j^2\right]$$

$$M_{\dot{h}_1} = \frac{-qS}{VI_Y}\left[\sum_{j=1}^{4} \left(C_{L_\alpha}\right)_j \, \bar{x}_j \, d_{1,j}\right] 57.3$$

$$M_{h_1} = \left\{\frac{qS}{I_Y}\left[\sum_{j=1}^{4} \left(C_{L_\alpha}\right)_j \, \bar{x}_j \lambda_{1,j}\right] + \frac{T}{I_Y}\left(\bar{x}_T \lambda_{1,T} - d_{1,T}\right)\right\} 57.3$$

$$M_{\dot{h}_2} = \frac{-qS}{VI_Y}\left[\sum_{j=1}^{4} \left(C_{L_\alpha}\right)_j \, \bar{x}_j \, d_{2,j}\right] 57.3$$

$$M_{h_2} = \left\{\frac{qS}{I_Y}\left[\sum_{j=1}^{4} \left(C_{L_\alpha}\right)_j \, \bar{x}_j \, \lambda_{2,j}\right] + \frac{T}{I_Y}\left(\bar{x}_T \lambda_{2,T} - d_{2,T}\right)\right\} 57.3$$

$$M_{\dot{h}_3} = \frac{-qS}{VI_Y}\left[\sum_{j=1}^{4}\left(C_{L_\alpha}\right)_j \bar{x}_j\, d_{3,j}\right] 57.3$$

$$M_{h_3} = \left\{\frac{qS}{I_Y}\left[\sum_{j=1}^{4}\left(C_{L_\alpha}\right)_j \bar{x}_j \lambda_{3,j}\right] + \frac{T}{I_Y}\left(\bar{x}_T \lambda_{3,T} - d_{3,T}\right)\right\} 57.3$$

$$M_\delta = \frac{qS}{I_Y}\left(C_{L_\delta}\right)_j \bar{x}_\delta + \frac{F_\delta \bar{x}_\delta}{I_Y}\, 57.3$$

APPENDIX B

GYRO ERROR STUDY

Although the study conducted for this paper included only motion in the pitch plane, gyro-induced errors in all three planes were studied.

The roll-datum drift ϵ_{ϕ} can be given by

$$\epsilon_{\phi} = \int_0^t k_{1\phi}\, dt + \int_0^t Ak_{2\phi}\, dt \tag{13}$$

where k_1 is the steady wander rate in radians/sec, k_2 is the mass-unbalance wander rate in radians/sec per ft/sec^2, and A is the apparent acceleration along the axis.

The yaw and pitch wander errors (ϵ, ψ, and θ) are given by

$$\epsilon_{\psi\theta} = \int_0^t k_{1\psi\theta}\, dt + \int_0^t k_{2\psi\theta}B\, dt \tag{14}$$

where B is the apparent acceleration normal to the missile axis.

To determine the errors that might be expected, the following assumptions were made:

(1) The apparent acceleration along the axis can be given by

$$A = \frac{T}{m} - \frac{\bar{q}SC_{D_o}}{m} \tag{15}$$

where C_{D_o} is the zero lift-drag coefficient.

(2) The apparent acceleration normal to the axis can be given by

$$B = \frac{L}{m} \sec \alpha = \frac{\bar{q}SC_{N_\alpha}\alpha}{m} \tag{16}$$

where C_{N_α} is the variation of normal-force coefficient with angle of attack.

(3) The angle-of-attack variation program consistent with a controls-locked zero-lift trajectory plus an additional degree of angle of attack attributed to various misalinements would be a conservative estimate.

Conservative values for the steady-wander and mass-unbalance rates for typical attitude gyros after a short period of vibration are 8°/hr and 8°/hr/g. By using these numbers and solving equations (13) and (14) based on trajectory data obtained from references 3 and 4, the roll datum can be expected to shift 0.4° and the pitch and yaw data to shift 0.1° each.

REFERENCES

1. J. B. Rea Co., Inc.: Aeroelasticity in Stability and Control. WADC Tech. Rep. 55-173, U.S. Air Force, Mar. 1957.

2. Harris, Jack E.: Analytical Investigation of an Adaptive Flight-Control System Using a Sinusoidal Test Signal. NASA TN D-909, 1961.

3. Smith, C. L.: Scout System Design Report. Supplement I - Basic System Design Data. R-ED 11122, Honeywell Aero. Div., Jan. 31, 1961.

4. Trujillo, T. A.: Scout System Design Report. Supplement II - Evaluation of First-Stage Control System for Fourth Vehicle and Increased Payload Lift Configurations. R-ED 11123, Honeywell Aero. Div., Feb. 3, 1961.

TABLE I.- SYSTEM TRANSFER FUNCTIONS

(a) Transfer functions for the servoactuator, the attitude gyroscope, and the compensating network

Transfer function	Numerical equivalent
Servoactuator	
$K_2G_2(s)$	$K_2 \frac{31}{s + 31}$
Attitude gyroscope	
$K_4G_4(s)$	$K_4 \frac{250}{s + 250}$
Compensating network	
$K_1G_{1,1}(s)$	$K_1 \frac{1914(s + 0.5)}{(s + 29)(s + 33)}$
$K_1G_{1,2}(s)$	$K_1 \frac{957(s + 1)}{(s + 29)(s + 33)}$
$K_1G_{1,3}(s)$	$K_1 \frac{478.5(s + 2)}{(s + 29)(s + 33)}$
$K_1G_{1,4}(s)$	$K_1 \frac{191.9(s + 0.5)(s + 1)}{(s + 29)(s + 33)(s + 0.1)}$

TABLE I.- SYSTEM TRANSFER FUNCTIONS - Concluded

(b) Airframe transfer functions

Mach number	Dynamic pressure, lb/sq ft	Time after launch, sec	$K_3G_3(s)$
0.25	100	5	$\frac{0.5449(s + 0.312)(s^2 + 1.374s + 366)(s^2 + 0.494s + 1930)(s^2 + 0.234s + 7350)}{s(s^2 + 0.38s + 0.251)(s^2 + 1.068s + 372)(s^2 + 1.098s + 1937)(s^2 + 2.2s + 7360)}$
.90	980	15	$\frac{0.8947(s + 0.158)(s^2 + 1.718s + 352)(s^2 + 0.734s + 2120)(s^2 + 0.548s + 7750)}{s(s^2 + 0.468s + 4.465)(s^2 + 1.37s + 379)(s^2 + 1.264s + 2130)(s^2 + 2.4s + 7800)}$
3.0	3,200	32.5	$\frac{1.235(s + 0.105)(s^2 + 2.06s + 279)(s^2 + 1.10s + 2470)(s^2 + 1.06s + 8760)}{s(s - 0.439)(s + 0.782)(s^2 + 1.40s + 346)(s^2 + 1.314s + 2490)(s^2 + 2.52s + 8840)}$
4.0	2,400	40	$\frac{0.774(s + 0.037)(s^2 + 1.934s + 340)(s^2 + 2.56s + 2730)(s^2 + 1.508s + 9890)}{s(s^2 + 0.176s + 0.637)(s^2 + 1.270s + 376)(s^2 + 2.68s + 2725)(s^2 + 2.60s + 9930)}$

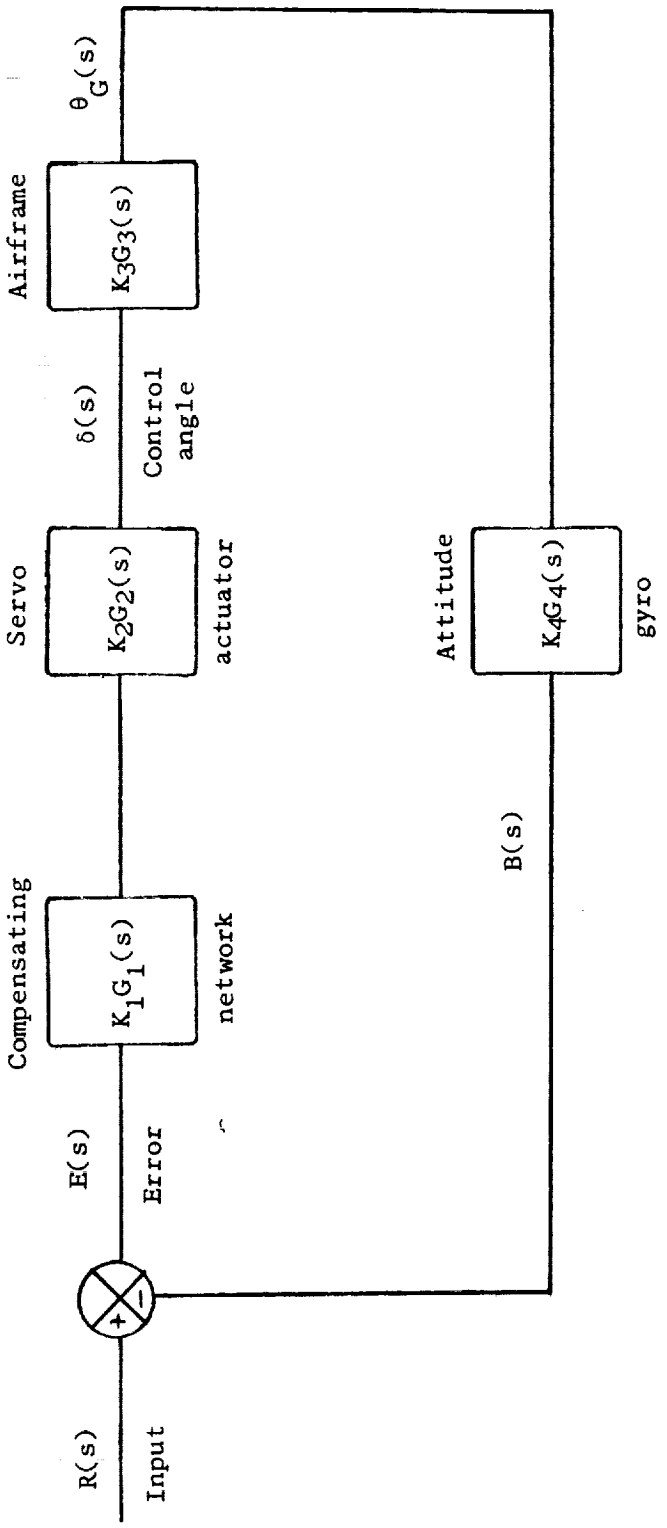

Figure 1.- Block diagram of control system.

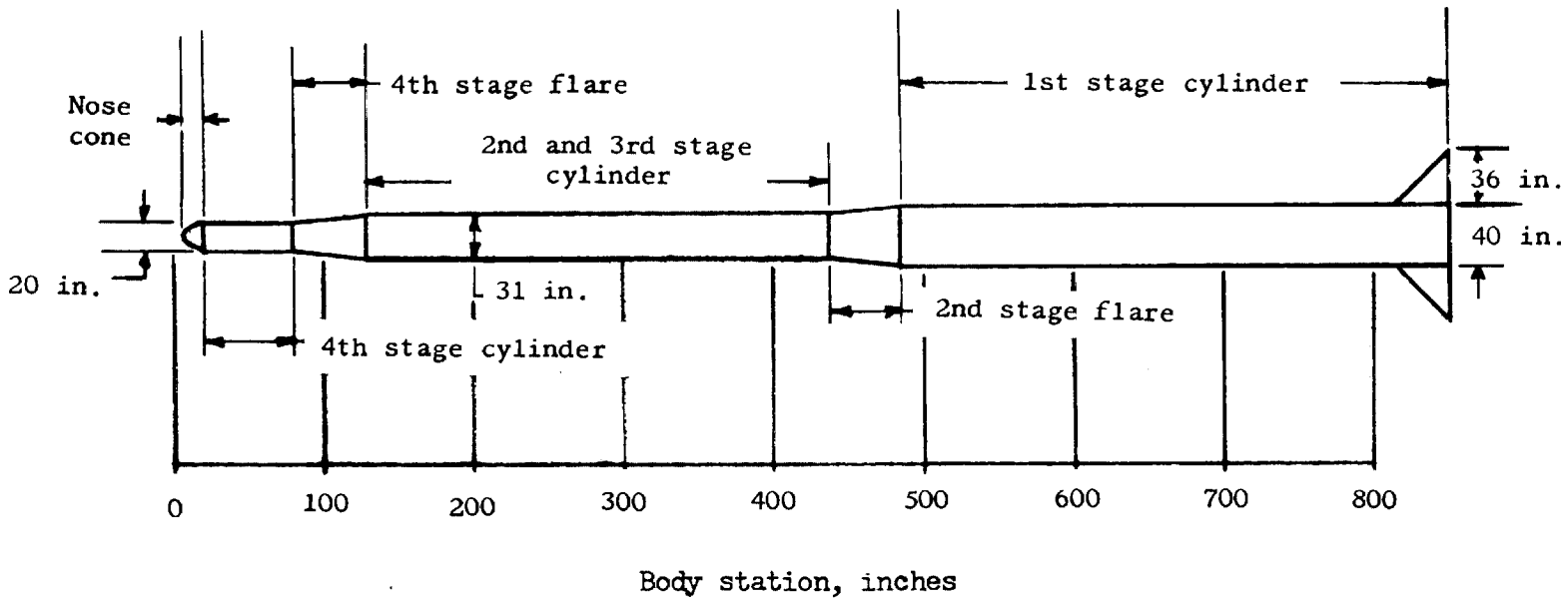

(a) Body dimensions and nomenclature.

Figure 2.- Missile characteristics and axes system.

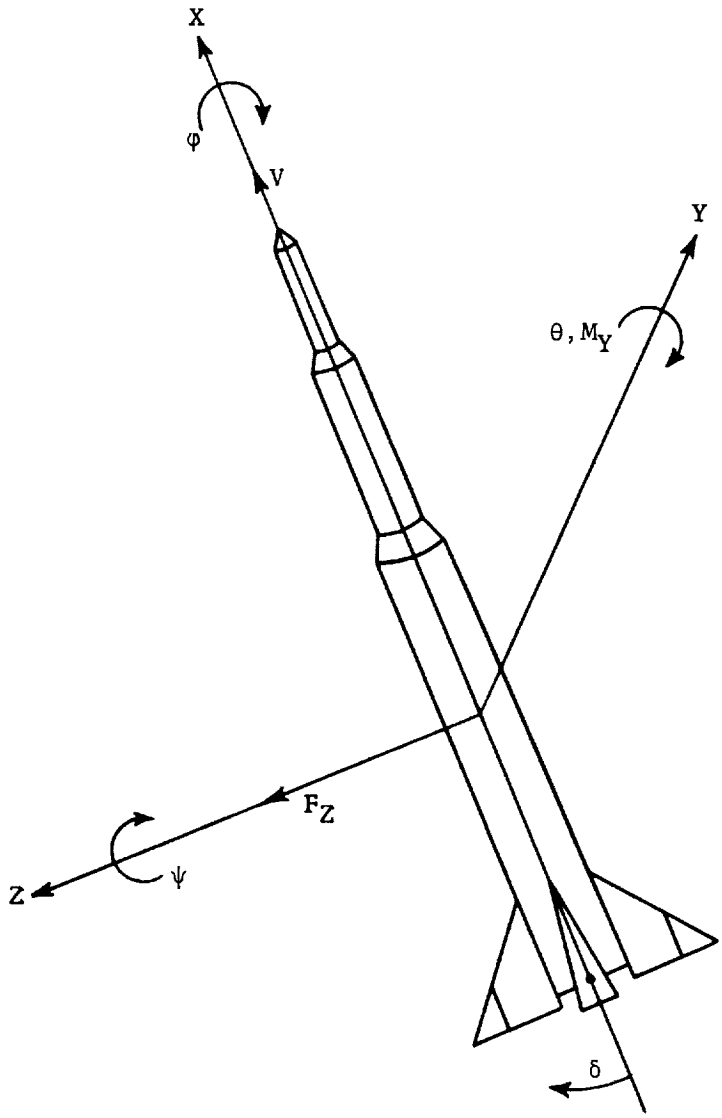

(b) Body-axis system employed with positive direction of forces, moments, and displacements shown.

Figure 2.- Concluded.

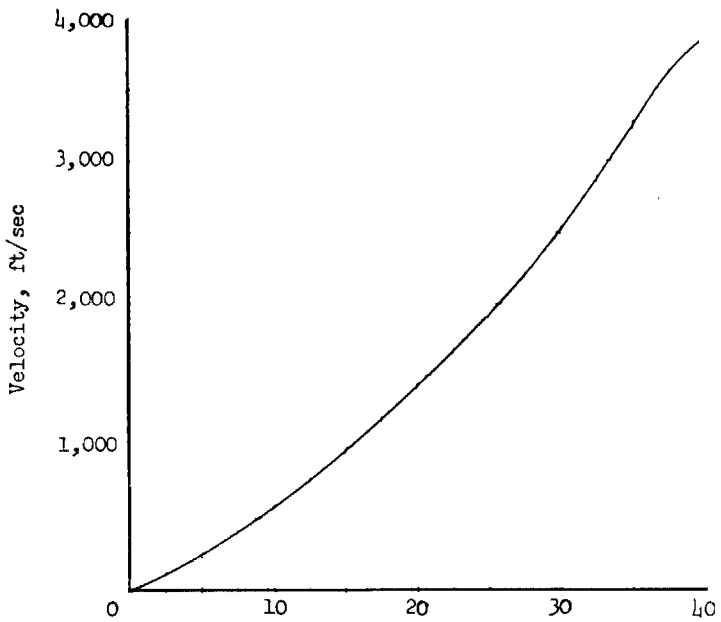

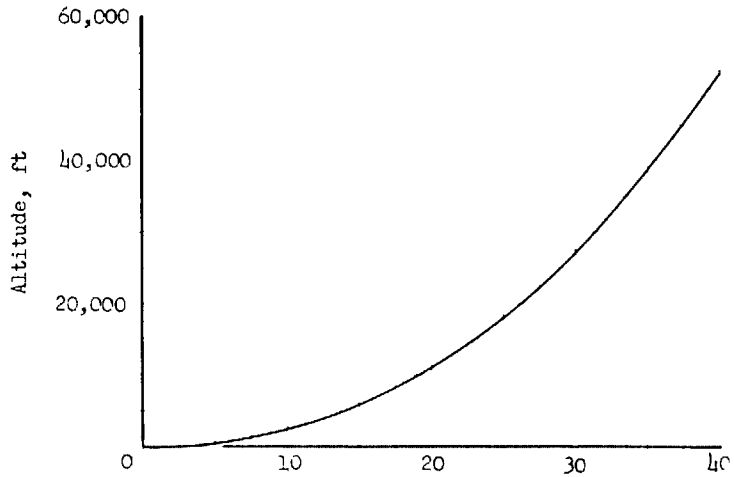

Figure 3.- Reference trajectory parameters. Launch angle, 80°.

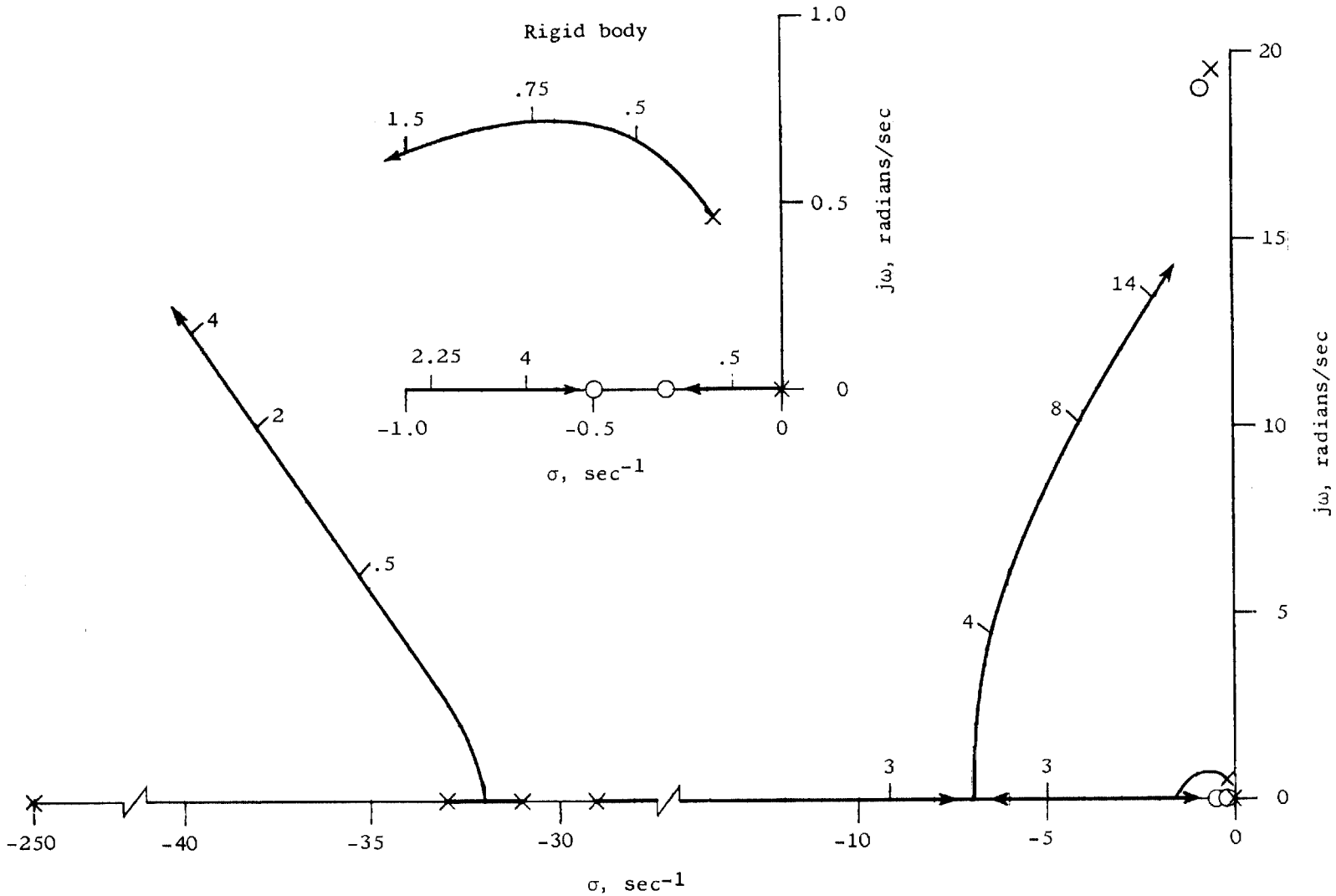

(a) Mach number, 0.25; dynamic pressure, 100 lb/sq ft; time after launch, 5 seconds.

Figure 4.- Root loci of pitch-attitude control system with network $G_{1,1}(s)$.

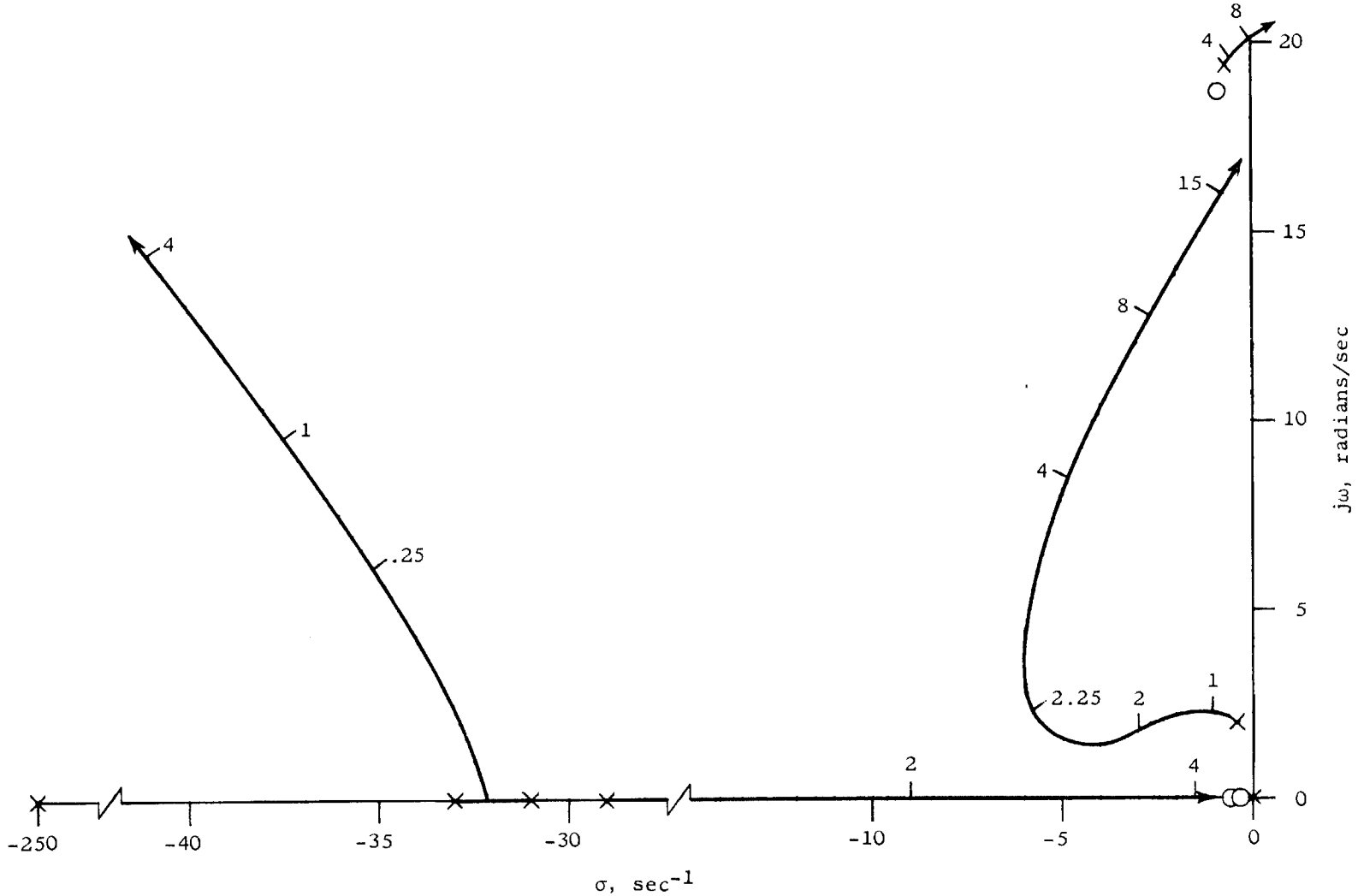

(b) Mach number 0.90; dynamic pressure, 980 lb/sq ft; time after launch, 15 seconds.

Figure 4.- Continued.

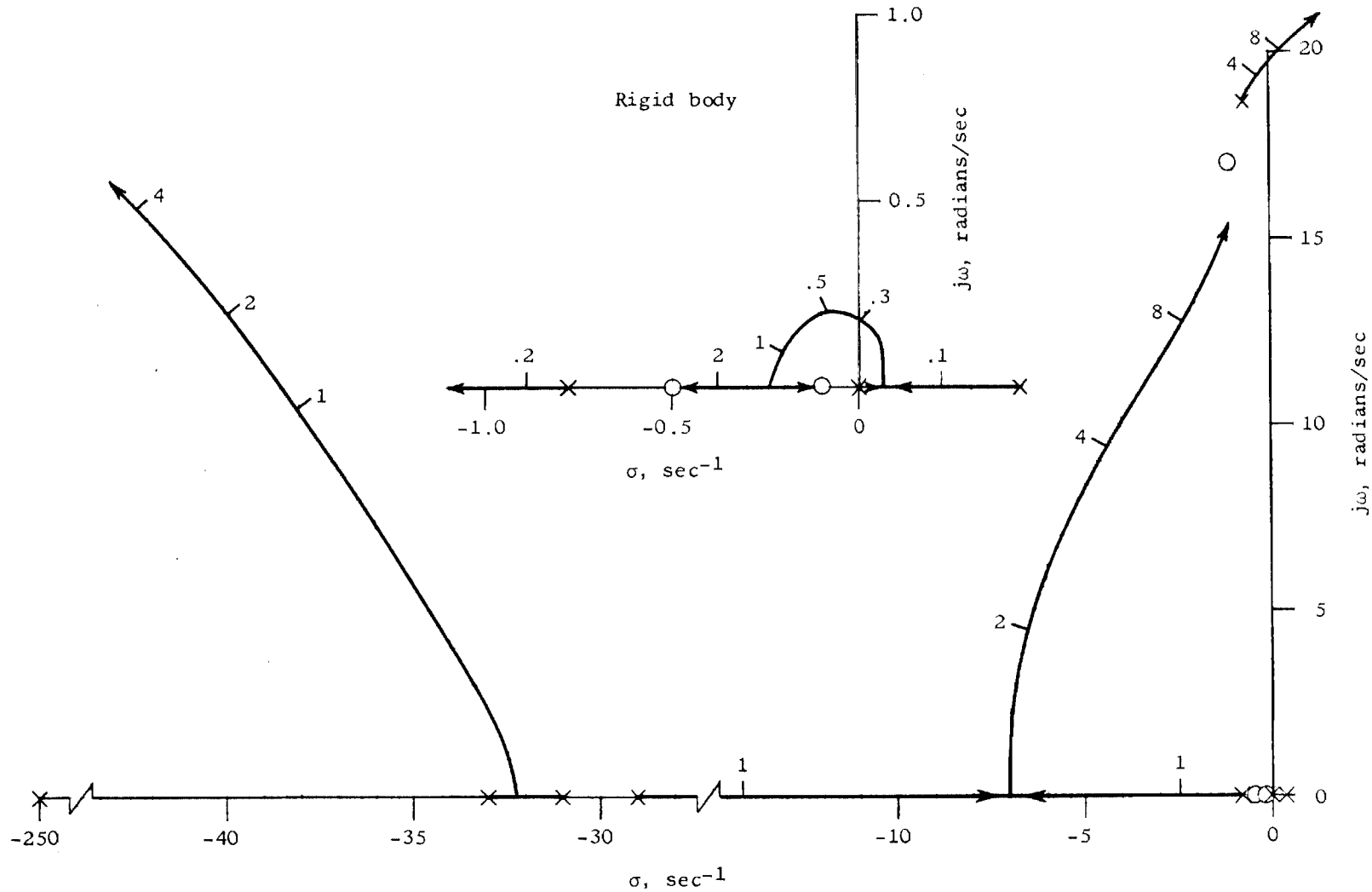

(c) Mach number, 3.0; dynamic pressure, 3,200 lb/sq ft; time after launch, 32.5 seconds.

Figure 4.- Concluded.

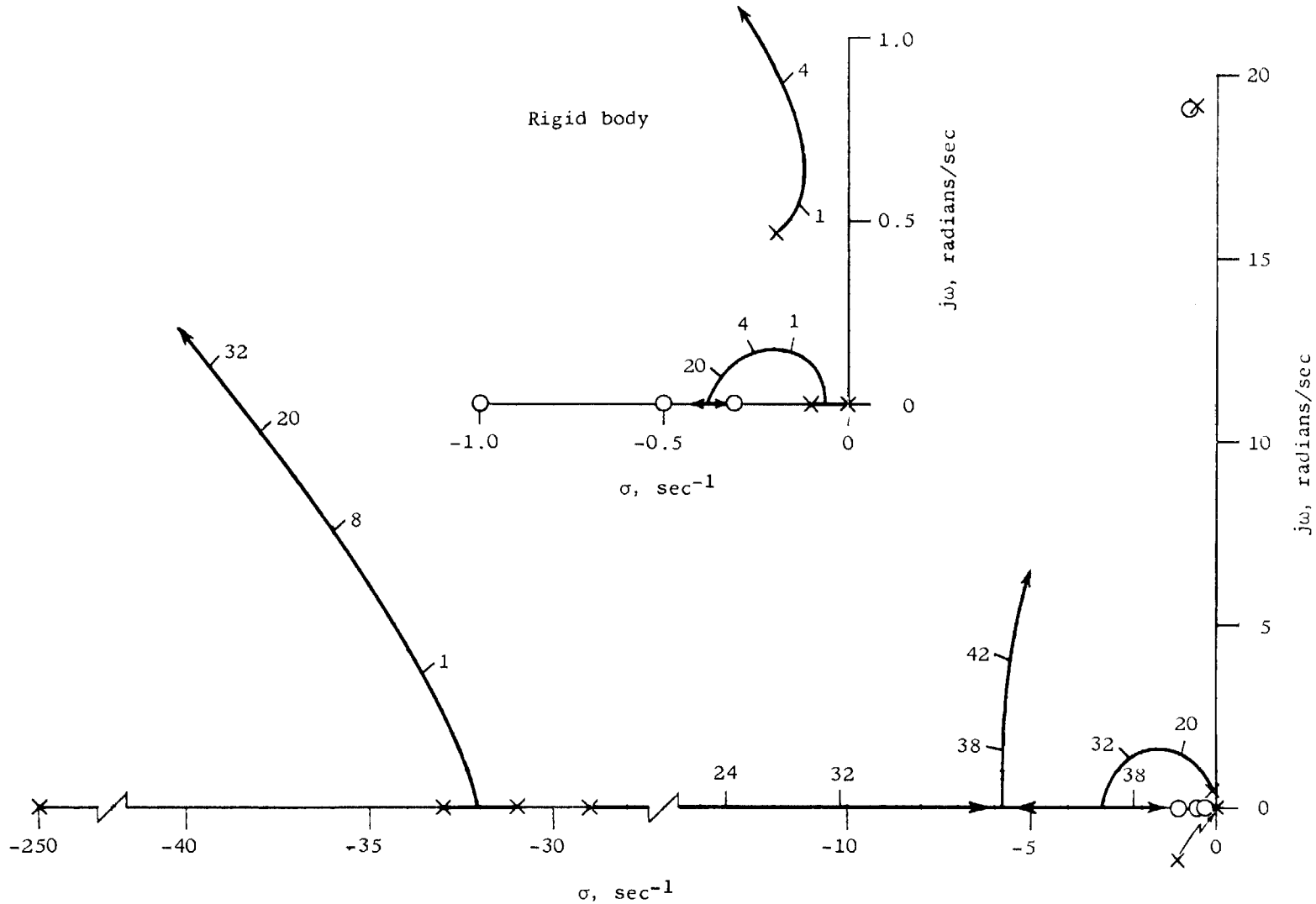

(a) Mach number, 0.25; dynamic pressure, 100 lb/sq ft; time after launch, 5 seconds.

Figure 5.- Root loci of pitch-attitude control system with network $G_{1,4}(s)$.

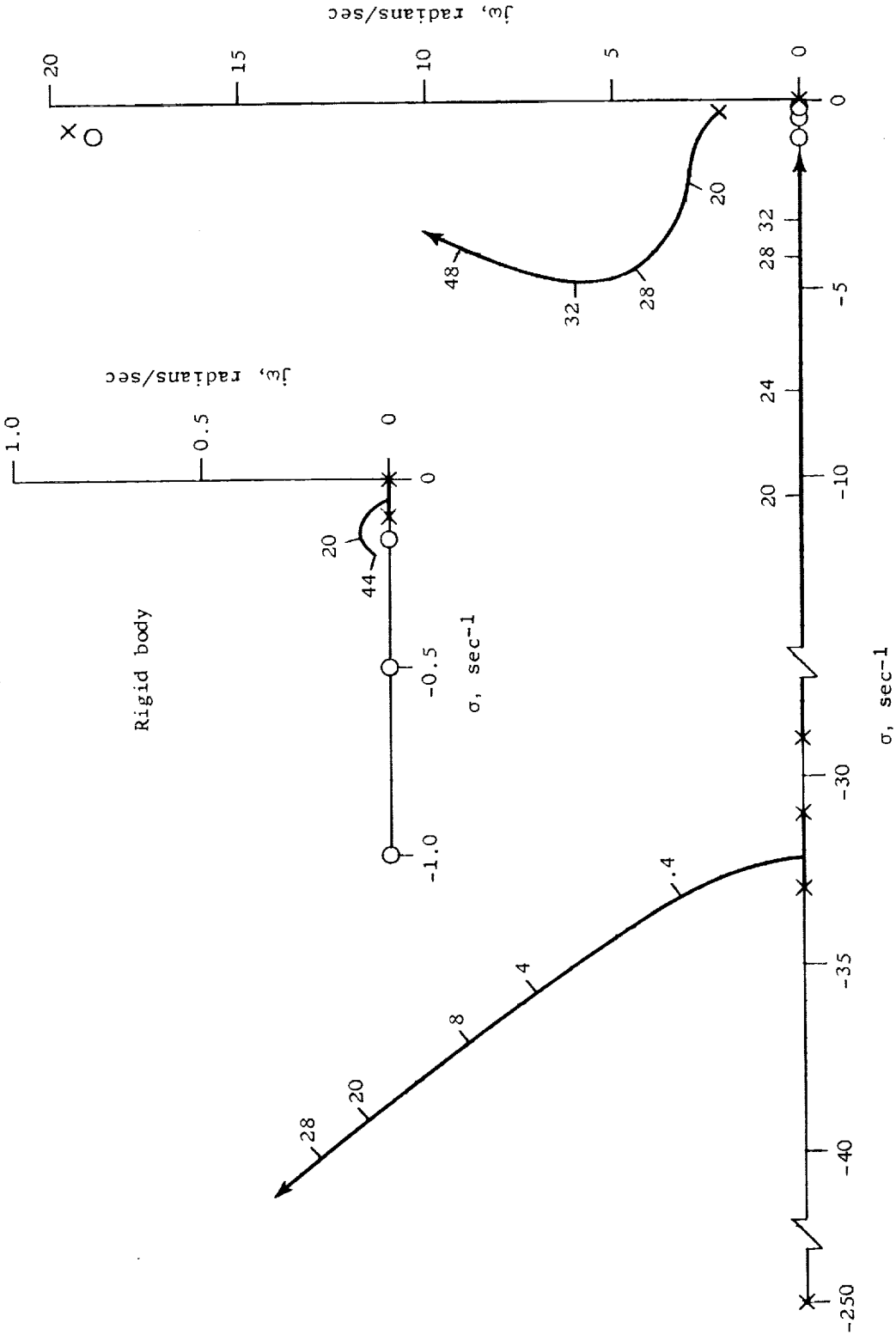

(b) Mach number, 0.90; dynamic pressure, 980 lb/sq ft; time ater launch, 15 seconds.

Figure 5.- Continued.

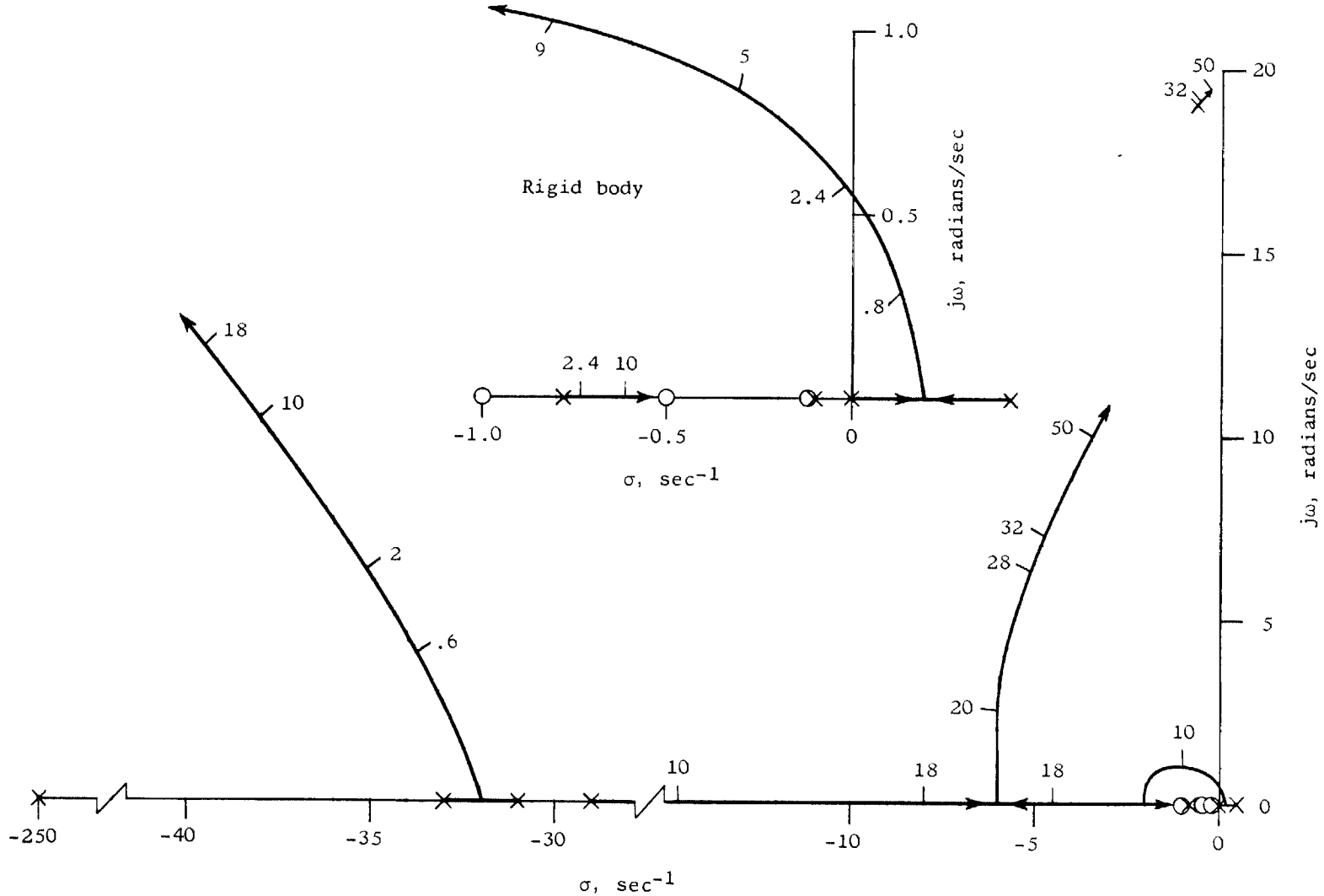

(c) Mach number, 3.0; dynamic pressure, 3,200 lb/sq ft; time after launch, 32.5 seconds.

Figure 5.- Concluded.

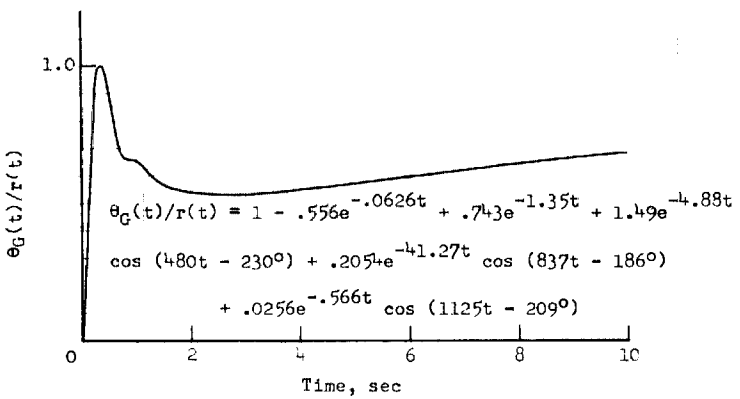

Command input 15 seconds after launch

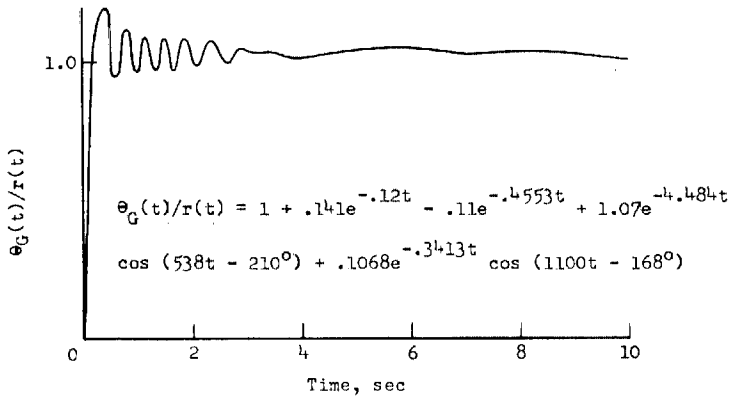

Command input 32.5 seconds after launch

(a) Network $G_{1,1}(s)$; loop gain = 4.

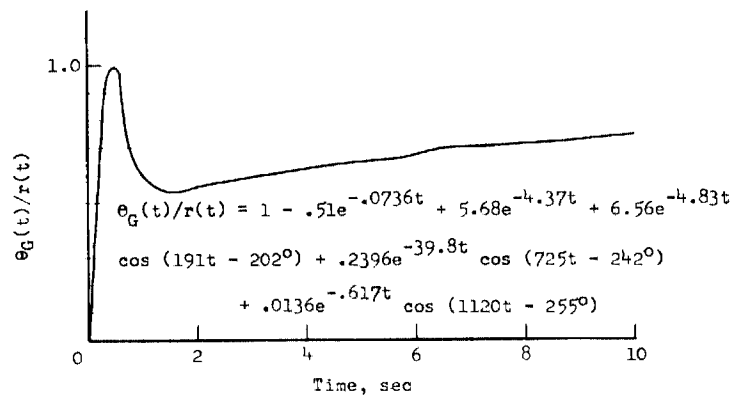

Command input 15 seconds after launch

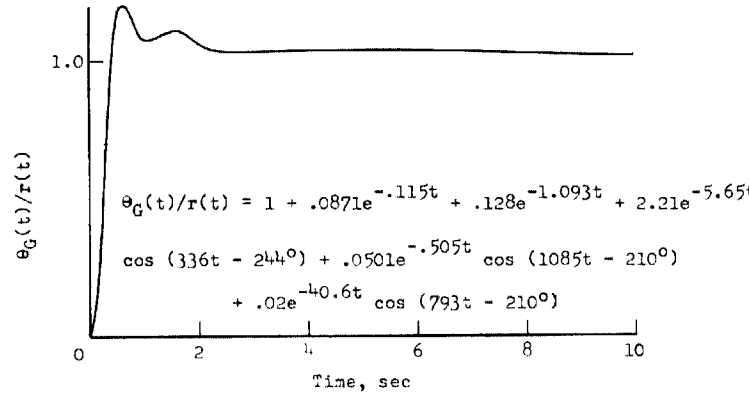

Command input 32.5 seconds after launch

(b) Network $G_{1,2}(s)$; loop gain = 5.

Figure 6.- Pitch-attitude time response to a step command input.

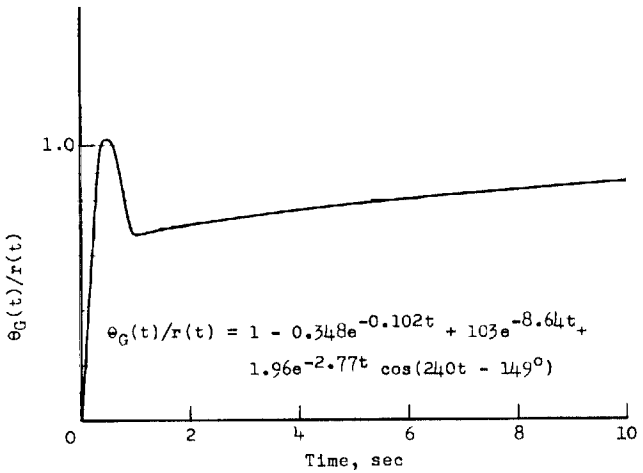

Command input 15 seconds after launch

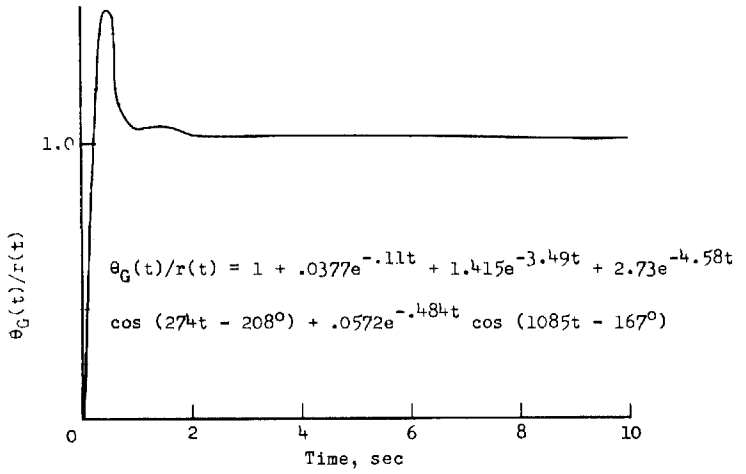

Command input 32.5 seconds after launch

(c) Network $G_{1,3}(s)$; loop gain = 10.

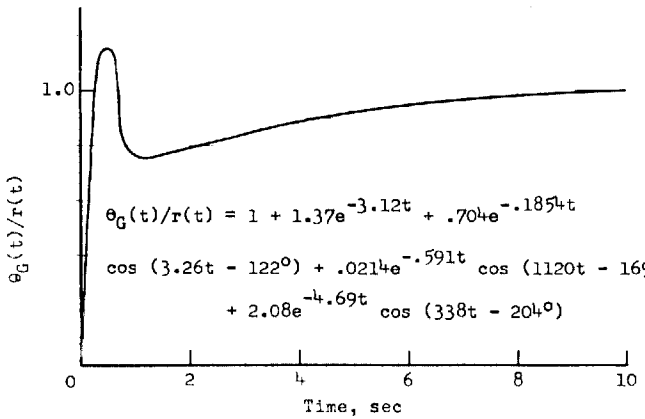

Command input 15 seconds after launch

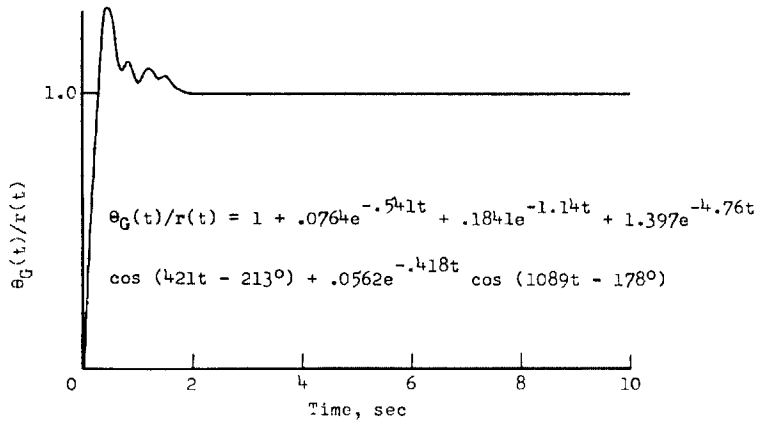

Command input 32.5 seconds after launch

(d) Network $G_{1,4}(s)$; loop gain = 32.

Figure 6.- Concluded.

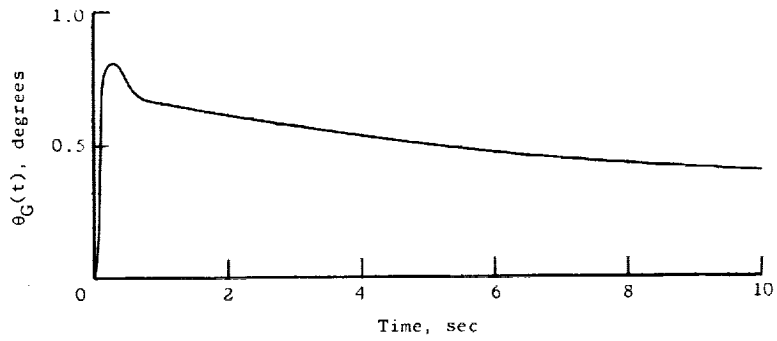

(a) Network $G_{1,1}(s)$; time after launch; 15 seconds; loop gain = 4.

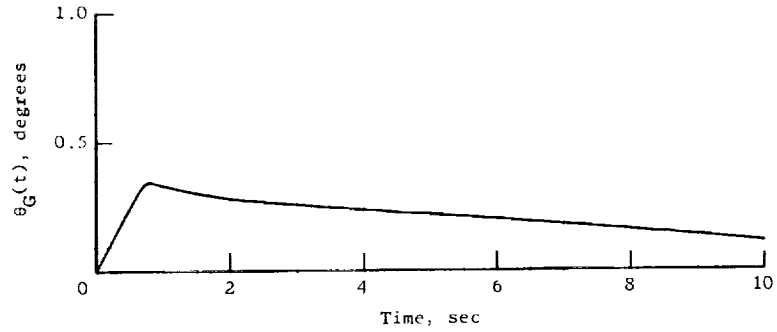

(b) Network $G_{1,3}(s)$; time after launch, 15 seconds; loop gain = 10.

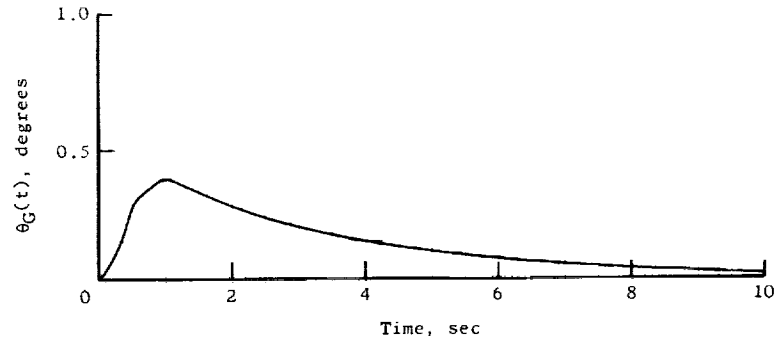

(c) Network $G_{1,4}(s)$; time after launch, 15 seconds; loop gain = 32.

Figure 7.- Transient-response curves of the change in attitude due to a unit step disturbance.

NASA-Langley, 1963 L-3202